Proceedings of 2004 Korea-Japan Joint Seminar
on Particle Image Velocimetry
POSTECH, Korea, Dec. 9 - 10

PIV Analysis of a Pulsating Flow through a Square Channel

Tetsuo SAGA, Toshiyuki UEDA and Nobuyuki TANIGUCHI

Institute of Industrial Science,
The University of Tokyo
4-61-1, Komaba, Meguro-ku, Tokyo, 153-8505, Japan
saga@iis.u-tokyo.ac.jp

Abstract: The effects of pulsation in a pulsating flow through a rectangular channel have been investigated by Particle Image Velocimetry in both laminar and turbulent flow conditions. PIV results on a square channel (aspect ratio:1) have been reported on the cases of Reynolds number Re=80 in laminar and Re=8800 in turbulent region. For both in the laminar and turbulent regions, the influence of the pulsation onto the magnitude changes of the average velocity was negligible. In the turbulent region, the magnitude profiles of the stream-wise pulsating component obtained by the theoretical analysis based on the Stokes analogy were slightly different from the experimental ones due to the influence of the turbulent viscosities onto the pulsating flows.

Keywords: PIV, Pulsating flow, Square channel, Velocity profile, Viscous sub-layer

1. Introduction

The flow fields having periodical pressure pulsations are widely seen ranging from the engineering piping system such as reciprocal compressor or heat transfer devices and the medical and biological piping system such as blood flow or breathing flow systems. Pulsation produced in engineering piping system produces cracks due to fatigues and decreases the compression efficiencies of the compressors, and produces uncertainties in flow rate measurements. Further, it is related to the injuries on the blood pipe in living bodies. Making use of the results obtained by analyses and predictions on those kinds of pulsating flow phenomena to designs, and constructing a database on the pulsating blood flow phenomena are useful for both engineering and medical applications.

There have been many reports on pulsating flows using numerical analyses for wide range of engineering applications [1][2]. For the case of low Reynolds region, the Stokes analogy is applicable. A theoretical analysis has been carried out for the pulsating flow in a rectangular duct by introducing the Stokes analogy in which the gradient of the pulsating pressure has been considered[3]. Womersly[4] made a theoretical analysis on the pulsating flow in a circular pipe.

In the mean time, there have been many experimental results on pulsating flows. Tardu et al.[5] carried out experiments on the turbulent channel flow with large-amplitude velocity oscillations. Ohmi et al. [6] reported on the critical Reynolds numbers on the pulsating flows in rectangular ducts in which transitions to turbulence was discussed in detail.

More recently numerical analyses have been carried out in turbulence region. Scotti et al. [7]

carried out a numerical simulation on turbulent pulsating channel flow with LES. They investigated the influences of pulsations onto the turbulent properties under various frequency conditions. Further, they investigated the inverse effects of the turbulence perturbations onto the momentum transfer in the pulsating boundary layer (Stokes layer) under various non-dimensional angular frequencies.

Since the pressure pulsating flows appear in various applications, numerical prediction on those flows is a very useful tool for understanding of the physics of the flows. However, it is strongly recommended to develop a definitive measurement technique for the verification of those numerical methods.

Nowadays, the field-wise measurement method, PIV (Particle Image Velocimetry) [8], is replacing the conventional point-wise measurements methods such as Hot Wire Anemometer and LDV (Laser Doppler Velocimeter). This is not only because the data obtained by PIV provide instantaneous spatial distribution of velocity vectors and make the researchers understand easily the physics of the flows, but because the most accurate experimental results can be obtained by attaining optimal PIV experiments.

Comparison of data obtained by the most advanced numerical analysis with those obtained by the highest experimental method is becoming crucial for the most advanced researches and developments in science and engineering. In this study, the pulsating flow in a square channel known as one of the representative rectangular ducts is experimentally investigated for the case of laminar and turbulent flow regions, in which the influence of the pulsation onto the time averaged velocity profiles and the influence of the turbulence perturbations onto the pulsating boundary layer are quantitatively evaluated. Further, experimental and numerical analyses results are compared and evaluated. For the laminar flow region the experimental results are compared with those of theoretical analysis made by Fan et al. [3] and with those of LES calculation carried out by Tominaga et al. [9], and their agreements is validated through comparison. For the turbulent flow region the experimental results are compared with the analytical results and LES results, through which the numerical prediction is validated.

2. Nomenclatures

$2a$ width of the square channel

D_h hydraulic radius $\equiv 4ab/(a+b)$, here $a=b$

L length of test section

u, v, w : velocity components of x, y, z directions

Re Reynolds number $\equiv u_{bulk} D_h / \nu$

Re_{osc} Pulsating Re number $\equiv \overline{u_1} D_h / \nu$

Re^*_{os} Reynolds number based on the Stokes layer thickness of boundary $\equiv \overline{u} l_s / \nu$

u_{bulk} average velocity in bulk

u_τ wall friction velocity

A velocity ratio $\overline{u_1} / u_{bulk}$

t time

f frequency of pulsating flow

ω angular frequency of pulsating flow

ω_0 non-dimensional angular frequency $\equiv D_h / 2\sqrt{\omega/\nu}$

ω^+ forcing frequency in wall unit $\equiv \omega\nu / u_\tau^2$

l_s thickness of pulsating boundary layer or Stokes layer thickness $\equiv \sqrt{2\nu/\omega}$

R cross-correlation coefficient

P, p pressure

μ viscosity coefficient

ν kinetic viscosity coefficient

$_0$ flow velocity, average component of pressure gradient

$_1$ flow velocity, pulsating component of pressure gradient

$_{center}$ center of channel pipe

$\overline{()}, ()'$ time-averaged and fluctuating components

3. PIV experiment and numerical analysis

3.1 Pulsating flow fields

Fig. (1) and (2) show the square channel with the coordinate system (width of the square channel, $2a = 1.7 \times 10^{-2}[m]$ length of channel $L = 1.5[m]$, aspect ratio:1) that can be regarded as infinitive to channel direction compared to channel section. Eq. (1) presents the pressure gradient of the pulsation to the channel direction (x) and was used for the analysis.

$$\frac{dp}{dx} = P_0 + P_1 \sin \omega t \qquad (1)$$

Experiment was carried out under atmospheric temperature and pressure conditions. Working fluid is dried air and is supplied to the square channel after passing through a constant pressure regulator from the air compressor. The air is passed through a rectifying screen and a honeycomb installed in the upstream of the square channel and is introduced to the square channel with uniform velocity profiles. The square channel was made of transparent acrylic for PIV measurements and its measurement location was set at 1000mm from the inlet of the square

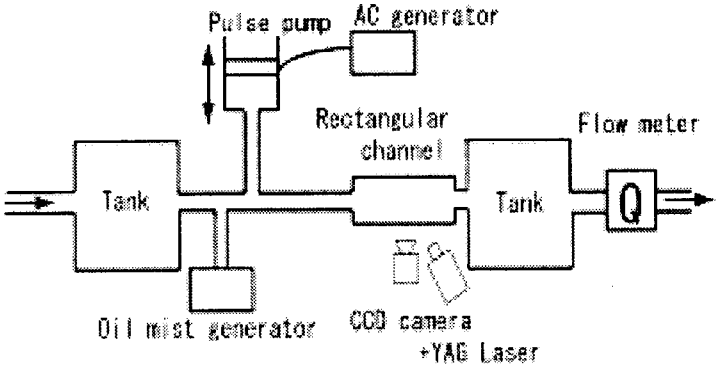

Fig.1 Schematic View of Experimental Apparatus

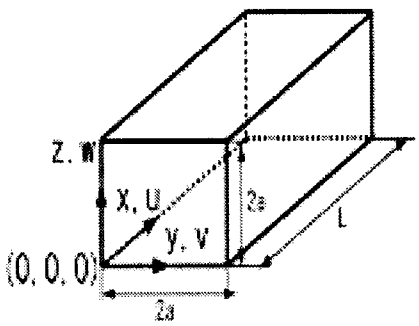

Fig.2 Square Channel and Its Coordinate System

channel. Pressure is pulsated with f=50Hz by the reciprocating pump installed on the upstream of the square channel and complete sine wave is produced. The serge tanks installed at both upstream and downstream of the square channel. The spatial phase difference between the pressure and the velocity becomes 90°, which implies that the antinode and the node of the pressure wave correspond to the node and the antinode of the velocity profile. The lengths between the upper and lower pipes of test section and the serge tanks were adjusted at a length at which the antinode (maximum) velocity profile was seen in the test section. In this study the wavelength of pulsation is 3.4 [m] which can be estimated from the sound velocity and the angular frequency of the pulsation under the atmospheric condition. Since the representative length of the channel width ($2a$) is $10^{-2}[m]$, the square channel can be regarded as an infinitive pipe.

3.2 PIV measurements

The PIV system constructed for this study consists of a Nd-YAG double pulsed laser (532[nm], 120[mJ]/pulse, repetition rate15Hz, pulse width 5[ns]), CCD camera(1008 x 1018 pixel, 8 bits, 30frame/[s]), a synchronizer (used for the synchronization of the pulsed laser and the camera) , and a workstation. The test section was set at 1000mm downstream region from the inlet of the transparent acrylic square channel. The tracer particles were injected at the upstream of the channel for PIV measurements as seen in Fig. 1. Since the flow field had strong unsteadiness, oil mist of which average diameter is P m were used as the tracers for PIV measurements to consider their traceability to the flows. The images were taken perpendicularly toward the illuminating plane visualized with the laser sheet of which thickness is 1mm (see Fig. 3). The distance between the camera and the test section was 350[mm], and the lens used was 50[mm] standard one and F-number was set to 5.6. The time interval of image capture, Δt was set 50[s] to 200[s] according to the mean velocity of the channel. The spatial resolution is 0.16 -0.16[mm] when the size of the searching window to be explained in the next section was set to 9 -9pixel .

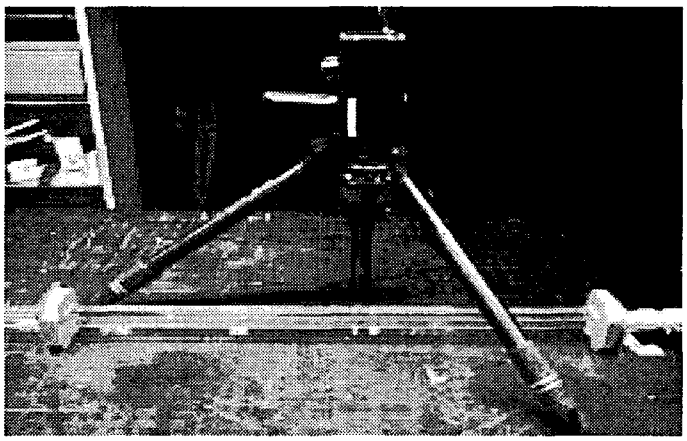

Fig.3 PIV measurement on a Square Channel

I

Image capturing was started by a trigger pulse generator of which signal was synchronized with the signal of the AC generator of the pulsating pump and with the PIV system. The time of image capturing was also shifted to a certain phase angle of the pulsating wave. One cycle of the pulsating wave was divided into 36 phase angles, and 50 sets of images at the same angle were used for the calculation of average velocity profiles. In case of non-pulsating flow condition, 300 sets of images were used to obtain the average velocity profiles.

3.3 Image analysis

In order to reduce the erroneous vectors that are produced from the calculation of sub-pixel resolution on the experimental images, a recursive cross-correlation method [10] was used in this study. Further, the prediction of the motions within the sub-pixel unit was made by the Continuous Wind-Shift Method [11] in order to avoid the peak locking of the particle's image. Below is the overall procedure for image analysis.

At first, a small search window is set on two consecutive images and the cross-correlation coefficients are calculated in this window using Eq. (2).

$$R(\Delta X,\Delta Y)=\frac{\sum_{i=1}^{N}\sum_{j=1}^{N}I(X_i,Y_i)I'(X_i+\Delta X,Y_j+\Delta Y)}{\sqrt{\sum_{i=1}^{N}\sum_{j=1}^{N}(I(X_i,Y_i))^2\sum_{i=1}^{N}\sum_{j=1}^{N}(I'(X_i+\Delta X,Y_j+\Delta Y))^2}} \tag{2}$$

Here, N represents the size of the interrogation window and I and I' mean the intensity distributions in the windows at the first and the second image, respectively. ΔX and ΔY imply the window's shifting to each axis of the photographical coordinate. The first size of the window is set to 32 ~32pixel and next to 9 ~9pixel for the recursive cross-correlation calculation to obtain the displacement in pixel unit. After this the displacement in sub-pixel level is calculated. Fig. 4 shows the intensity pattern (I'') in sub-pixel level and this value is obtained by using Eq. (3) in which weighted interpolation concept is embedded.

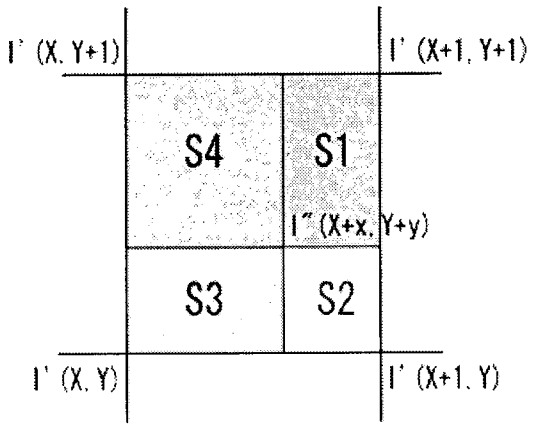

Fig4. Prediction of Sub-pixel Image Density

$$I''(X+x,Y+y)=S_1\times I'(X,Y)+S_2\times I'(X,Y+1)+S_3\times I'(X+1,Y+1)+S_4\times I'(X+1,Y) \tag{3}$$

Here, (X,Y) implies the displacement position which is obtained by the recursive cross-correlation method, and (x,y) implies the displacement position in sub-pixel unit. Again, the last cross-correlation coefficients are calculated on (X,Y) with the same $N\times N$ window size replacing I' with I'' in Eq. (2) . With this calculation the order of 0.01 pixel displacement is obtained (Window-Shift concept). Fig. 5 shows the measurement results with pixel unit and sub-pixel unit,respectively. In case of the calculation using the pixel intensity some wavy errors in the

velocity profile are seen in Fig. 5(a) due to the peak locking of the intensity. However, the results of sub-pixel calculation shows smooth velocity profile as seen in Fig. 5(b), which implies that the shift-window method adopted in this study is valid. In the mean while, the measurement uncertainty was estimated to 2.5% with 95% reliability against the local velocity of channel center.

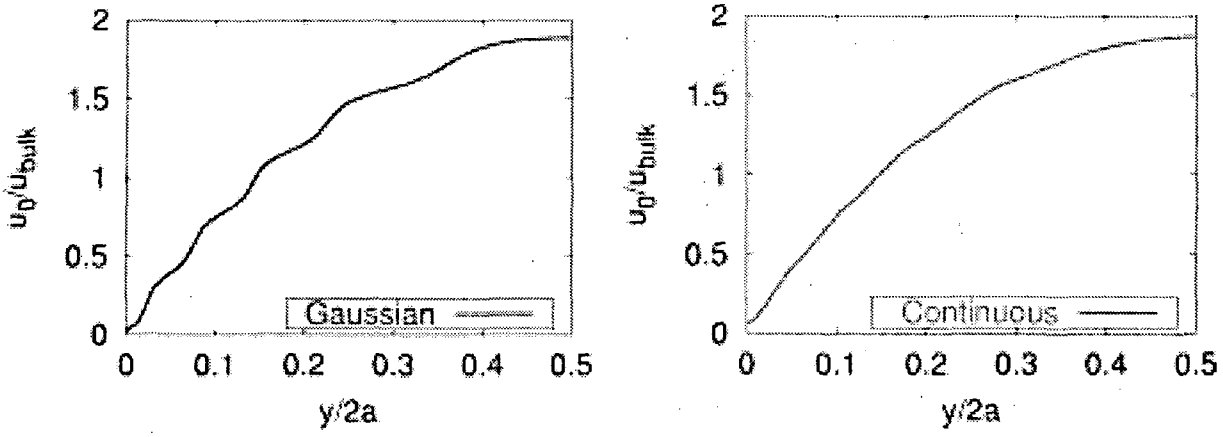

(a) Gaussian Fitting (b) Continuous Window – Shift

Fig .5 Reduction of Peak Locking Error

3.4 Numerical analysis

3.4.1 Numerical analysis of Stokes analogy[3]

In this section, the results of the theoretical analysis on the laminar flow (Re=80) are presented using those of Fan et al.[3] . In case of the infinitive square channel with steady and unsteady pressure gradient, the steady pressure gradient, $dp/dx = p_0$ and the unsteady pressure gradient, $dp/dx = p_1 \sin \omega t$ can be expressed in the form of Eq. (5) and Eq. (6), respectively.

Under a constant pressure gradient :

$$u(y,z) = -4ab\left(\frac{P_0}{\mu}\right)\frac{16}{\pi^2}\sum_{n=0}^{\infty}\sum_{m=0}^{\infty} \times \frac{(-1)^{m+n}\alpha}{(2m+1)^3(2n+1)+(2m+1)(2n+1)^3\alpha^2} \times \cos\frac{(2m+1)\pi}{2}y \times \cos\frac{(2n+1)\pi}{2}z \tag{5}$$

Here, $\bar{y} = y/a$ $\bar{z} = z/b$ and the aspect ratio of the square channel is $\alpha = a/b$.

Under a harmonically oscillating pressure gradient:

$$u(y,z) = -\frac{P_1}{\rho\omega}\frac{16}{\pi^2}\sum_{n=0}^{\infty}\sum_{m=0}^{\infty} \times \frac{(-1)^{m+n}}{(2m+1)(2n+1)} \times \cos\frac{(2m+1)\pi}{2}y \times \cos\frac{(2n+1)\pi}{2}z\{m,n\} \tag{6}$$

where, ψ is a dimensionless frequency parameter defined as $\psi = ab\omega/\nu$ and $\{m,n\}$ is an abbreviation as follows.

$$\{m,n\} = \{\frac{\psi(\pi^2/4)[(2m+1)^2/\alpha + (2n+1)^2\alpha]\cos\omega t + \psi^2 \sin\omega t}{\psi^2 + \pi^4/16[(2m+1)^2/\alpha + (2n+1)^2\alpha]^2}\}$$

In the laminar region the results obtained in the next sections was compared with the curve profiles figured out with Eq. (5) and Eq. (6). The subscript n at $\sum_n^\infty$ in the two equations was set to n=100.

3.4.1 Large eddy simulation[9]

Tominaga et al.[9] carried out a numerical simulation using a LES code in which incompressible Navier-Stokes equation was used as the governing equation for the general curvilinear coordinate system. Table 1 shows the LES code configurations.

Table 1 LES code configurations

Time Step	Fractional Step Method
Time Integration	Convection Term, 2nd order accuracy, Adams-Bashforth Method Non-convective Term, 2nd order accuracy, Crank-Nicolson Method
Space Discretization	2nd Central difference

Fig. 6 shows the grid system used for LES calculation. Irregular grid system on the Cartesian coordinate was used and the number of girds was 64 ~64 ~32 and its resolution was $\Delta x^+ = 22.8, \Delta y^+, \Delta z^+ = 0.589 - 17.9$ to each direction. The periodic boundary condition was used for the stream direction, and non-slip condition was used on the wall.

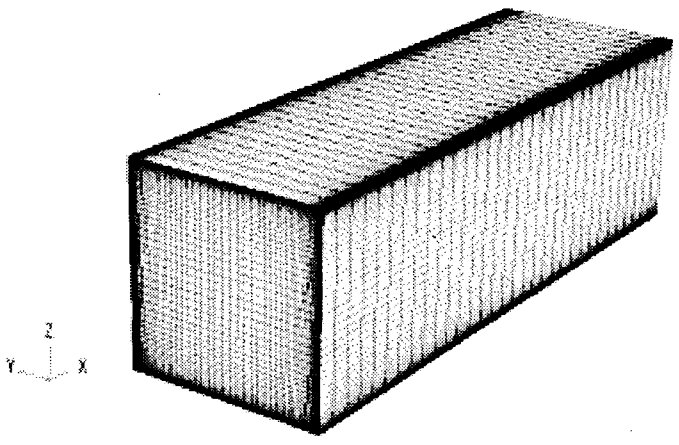

Fig.6 Grid of LES Analysis

4. Experimental results and discussion

In this chapter, comparison of the PIV results was made with the analytical results of Fan et al.[3] and the LES results of Tominaga et al.[9]. The characteristics of the pressure pulsating flow field were investigated and the validation of the numerical prediction was evaluated through the comparison.

The Reynolds numbers are Re=80 `8800 and the ones in case of pulsating flow are $Re_{os}$=320 `1800. The non-dimensional angular frequency is ω_0=38.4 f=50Hz and the thickness of the pulsating boundary layer l_s=0.313mm.

Here, the experimental results obtained in the laminar region with P_0=120(Pa/m) and Re=80, and the turbulent region with P_0=750(Pa/m) and Re=8800, were compared with those of the numerical analyses. Table 2 and 3 show the conditions for experimental and numerical analyses.

Table 2 Experimental conditions

Re	Re_{os}	A	ω_0	$P_1[Pa/m]$	$u_{bulk}[m/s]$
80	320	4.0	38.4	120	0.072
8800	1800	0.2	38.4	750	7.942

Table 3 Numerical analysis conditions

Re	Re_{os}	A	ω_0	$P_1[Pa/m]$	$u_{bulk}[m/s]$
80	400	2.64	38.4	166	0.072
8000	4500	0.45	38.4	1500	7.15

4.1 Data arrangements for comparisons of the results

In general, the velocity profile of u in the square channel can be a function of y as expressed in Eq. (7).

$$u(y) = u_0(y) + u_1(y)\sin(\omega t + \phi(y)) + u'(y) \tag{7}$$

Here, u_0 is the steady component, u_1 is the pulsating component, u' is fluctuating component, and ϕ is the phase delay of the pulsations. Further, u_1 was obtained by taking an average of u at each phase and taking the half value (1/2) of the difference between the maximum u_{max} and the minimum u_{min}. Fig. 7 shows the velocity profile of the pulsating flow in the measurement region at an instant (`=180deg). Since the velocity profiles of the stream-wise direction in the measurement region show homogeneous, the average velocity has been obtained by taking an arithmetic averaging with the velocities onto the mainstream direction as expressed in Eq. (8).

$$u(y) = \frac{1}{N}\sum_{i=1}^{N} u(x_i, y) \tag{8}$$

In case of pulsating flow, one cycle of the pulsating wave was divided into 36 phase angles, and 50 sets of images at the same angle were used for the calculation of average velocity profiles. In case of non-pulsating flow, 300 sets of images were used to obtain the average velocity profiles.

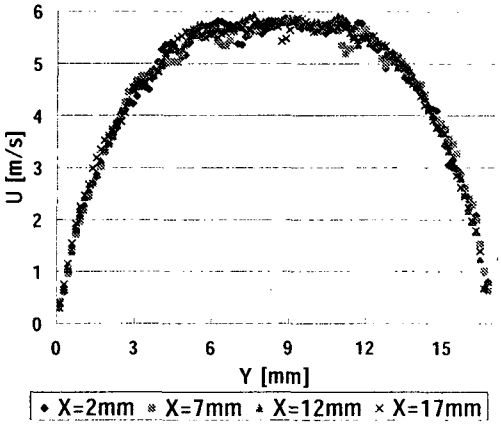

Fig.7 Instantaneous Velocity Distribution at the Measuring Region in the Channel Center Plane (Re=3700, A=0.3, ˜=180deg.)

4.1 Comparisons results on laminar flow region

In this section, the results of experiments and numerical analyses are compared for the case of laminar flow region (Re=80). Fig. 8(a) and 8(b) show the profiles of the average velocity (u_0) and the pulsating component (u_1) on the channel center plane, respectively. The experimental results (Exp.) were compared with those (Analysis) obtained by the theoretical analysis of Fan et al.[3] and those (Calc.) done by LES of Tominaga et al. [9].

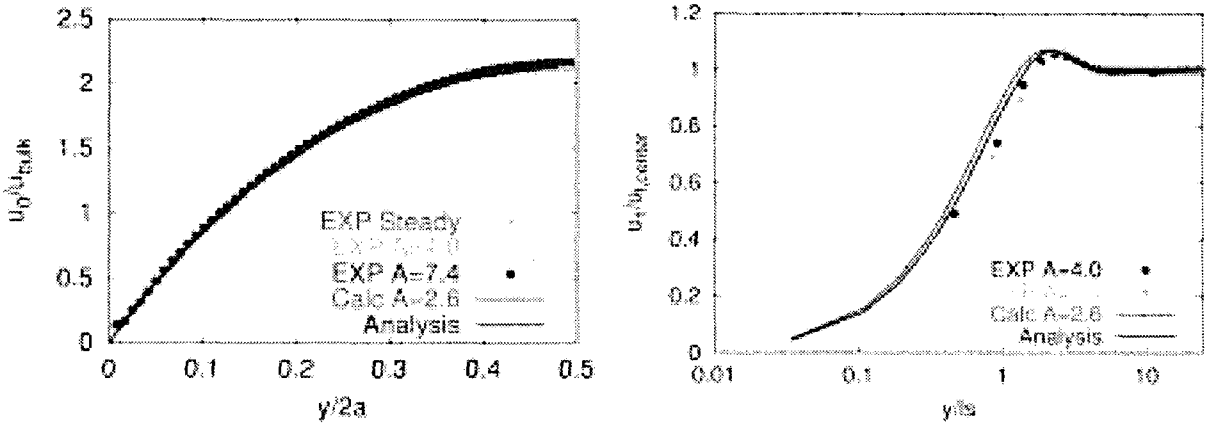

(a) Stream-wise Velocity

(b) Amplitude of Stream-wise Pulsating Velocity Component

Fig. 8 Profile of Velocity and its Amplitude (Re=80)

It can be said that a good agreement between the average velocity profiles on the stream-wise direction is seen for both steady and unsteady pressure gradient cases, and that the pulsating components do not influence the steady flow fields. Further, it is seen that the profiles of the average velocity and the pulsating component have good agreements along the stream-wise direction.

Fig. 9 shows the phase changes of the pulsating component (u_1) of the stream-wise velocity at

the center of the channel. It is seen that the phase of the pulsating velocity is advanced with $\pi/2$ against the phase of the pulsating pressure gradient (Pressure). It can be said that a good agreement between the velocity profiles obtained by the experiments (E) and the theoretical analyses (A) of Fan et al. is also seen.

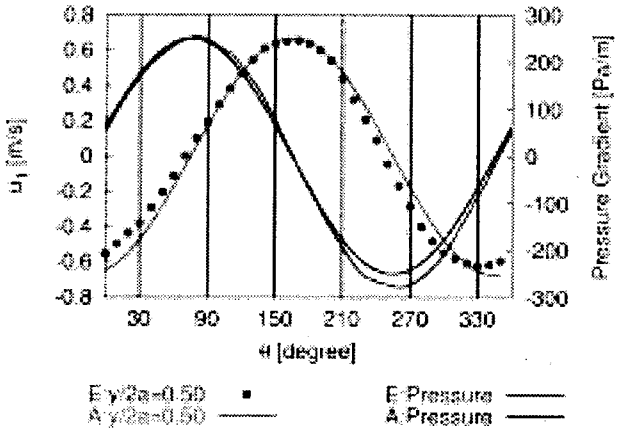

Fig.9 Change of Pressure and Stream-wise Velocity by Phase angle at the Center of Channel

Fig. 10 show the phase averaged velocity profiles along the span-wise axis of the center plane at the phases, θ =30, 90, 150, 270 and 300 deg. It can be said from this figure that the acceleration region is at the phase from θ =30, 90, 150 degrees and the deceleration region is at θ =270, 330 degrees. Further, it can be said that the patterns of the phase delay appear well near the wall and the profiles obtained by the experiments (E) and by the theoretical analyses (A) show nearly same patterns. With these, it can be said that the results obtained by the theoretical analysis present well enough the characteristics of the pulsating flows in the laminar region.

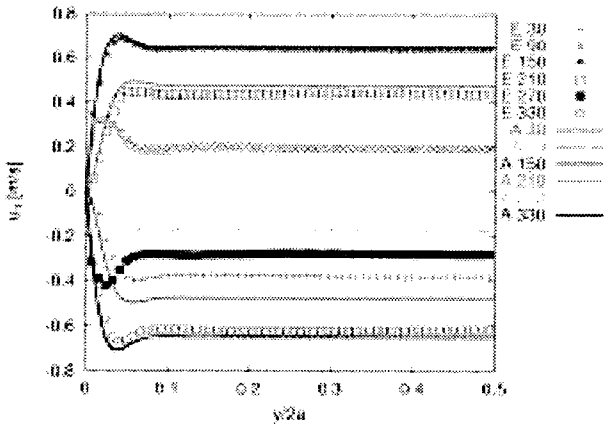

Fig.10 Change of Stream-wise Velocity along the Span-wise Axis of the Channel Center Plane

4.1 Comparisons results on turbulent flow region

In this section, the results of experiments and numerical analyses are compared for the case of turbulent flow region (Re=8,800). Fig. 11(a) and 11(b) show the profiles of the stream-wise steady component of velocity (u_0) and the pulsating component (u_1) on the span-wise axis of the center plane, respectively. As in the case of laminar flow, the experimental results (Exp.) were compared

with those of theoretical analysis of Fan et al.[3] and those of LES of Tominaga et al.[9]. It can also be said that a good agreement between the average velocity profiles on the stream-wise direction is seen for both steady (Exp. Steady) and pulsating pressure gradient cases (Exp. A=0.13, 0.2). The LES results on the steady pressure gradient case (Calc. Steady) and on the pulsating pressure gradient case (Calc. A=0.13, 0.2) show nearly similar curves each other. However, it can be seen that the LES results are about 8% bigger than those of experiments at the center of the channel. This overestimation of averaged stream-wise velocity was observed in LES of turbulent flow in 2D-channel that was calculated using 2nd order central differential scheme on a co-location grid system. It is expected that changing a differential scheme to higher order one or changing a grid to

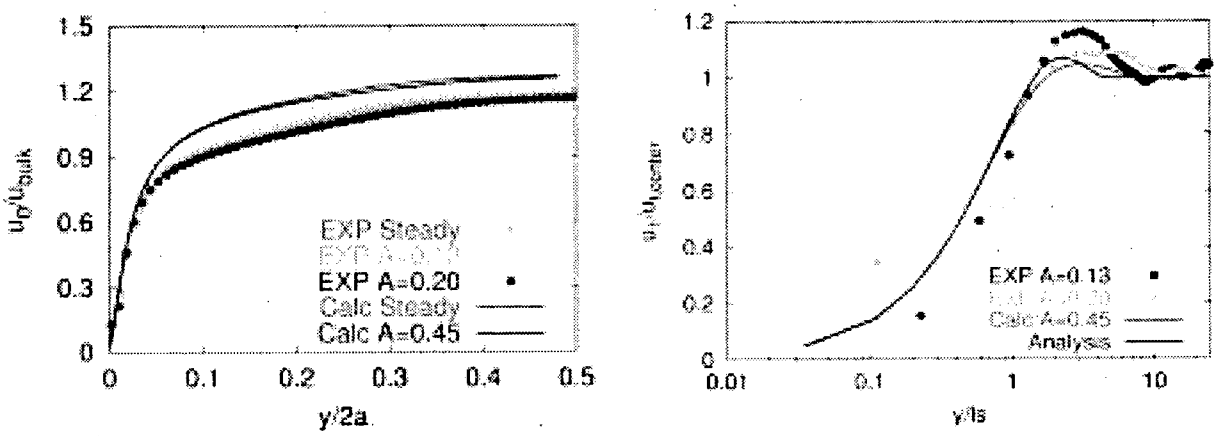

(a) Stream-wise Velocity (b) Amplitude Stream-wise Velocity Pulsation

Fig. 11 Profile of Stream wise Velocity and Its Amplitude (Re=8800)

the one with higher resolution will also reduce the overestimation. With these facts in the above, it can be said that the pulsation components do not influence the average velocity profiles under the present experimental conditions.

In the pulsating component of the stream-wise direction, it could be seen that the peak of the magnitude profile obtained by the experiments (Exp. A=0.13, 0.20) is farer than that obtained by the Stokes analogy (Analysis) as shown in Fig. 11(b). This phenomenon is due to the fact that the thickness of the pulsating boundary layer becomes thicker than that of the viscous sub-layer, which eventually produces the increasing effect of the thickness of the pulsating boundary layer due to turbulent viscosity. This tendency is qualitatively verified by the LES results (Calc.) made by Tominaga et al.[10]. The non-dimensional angular velocity $\omega^+ = 0.018$ at which the above phenomenon is seen as same as that $\omega^+ \leq 0.020$ reported by Scotti et al.[7] using LES and DNS, which support the validation of the experimental results in this study.

5. Conclusions

In this study, PIV analysis on the pulsating flow in a square channel (aspect ratio: 1) known as one of the representative rectangular ducts has been experimentally carried out for the case of laminar and turbulent regions.

Under the experimental conditions (Re=80 `8800 ÆP₁=120 `750[Pa/m] Æ$\omega_0 = 76.8$), the results were compared and validated with those of theoretical analyses and LES calculation. Followings are the summaries.

(1) In the laminar region, it has been verified that the velocity profiles obtained by the

experiments have shown well the general characteristics of the pulsating flow. Further, the experimental results showed good agreements on the stream-wise average velocity profiles with those obtained by the theoretical analysis and by LES for both steady and unsteady pressure gradient cases. It was also verified that the influence of the pulsation onto the magnitude changes of the stream-wise average velocity and pulsating components did not appear.

(2) In the turbulent region, it was verified from the PIV experiments and LES calculation that the influence of the pulsation onto the magnitude changes of the stream-wise average velocity did not appear. It was also verified that the magnitude profiles of the stream-wise pulsating component obtained by the theoretical analysis based on the Stokes analogy were slightly different from the experimental ones because the thickness of the pulsating boundary layer was increased due to the influence of the turbulences onto the pulsating flows.

The results obtained in this study were used for the design of flow passage of the gas flow meter.

Acknowledgement

The authors would like to thank Mr. Tominaga, T. (Ph. D student of the University of Tokyo), Professor .Oshima, M.(I.I.S., the University Tokyo) and Mr. Kobayashi, K.(Tokyo Gas Co. Ltd.) for their valuable discussion during this investigation.

References

(1) Gundogdu,M.Y., et al., "Present state of art on pulsatile flow theory (Part 1: Laminar and transitional flow regimes) ", JSME International Journal Series B, Vol.42, No.3, (1999),pp.384-397

(2) Gundogdu,M.Y., et al., "Present state of art on pulsatile flow theory (Part 2: Turbulent flow regime) ", JSME International Journal Series B, Vol.42, No.3, (1999), pp.398-410

(3) Fan,C., et al., "Unsteady, laminar, incompressible flow through rectangular ducts", B.-T., Z. Angew. Math. Phys.," Vol.16, (1965), pp.351-360

(4) Womersley, J. R., "Method for the calculation of velocity, rate of flow and viscous drag in arteries when the pressure gradient is known", J. Physiol.., Vol.127, (1955), pp.553-563

(5) Tardu, S. F., Binder, G. and Blackwelder, R.F., "Turbulent channel flow with large-amplitude velocity oscillations", J. Fluid Mech., Vol.267, (1994), pp.109-151

(6) Ohmi, M., et al., "Transition to turbulence in a pulsatile pipe flow. Part1 ; Waveforms and distribution of pulsatile velocities near transition region", Bulletin of the JSME, Vol.25, No.200, (1982),pp.182

(7) Scotti,A., Piomelli,U., "Numerical simulation of pulsating channel flow", Physics of Fluids, Vol.13, No.5, (2001), pp.1367-1384

(8) PIV Handbook, Ed. by Visualization Society of Japan, (2002), Morikita Shuppan

(9) Tominaga, T., Taniguchi, N., Ueda, T., Saga, T., "Numerical Simulation of Pulsating Flow through a Rectangular Channel", Proc. of 17 th Symposium on Numerical Fluid dynamics , D11-3,(2003)

(10)Hu, H., .Saga, T., Kobayashi, T., Taniguchi, N., Segawa, S., "Improve the spatial resolution of PIV results by using hierachical recursive operation", Proc. of 9 th International Symposium on Flow Visualization, (2000), pp137-(1-12)

(11)Gui, L., and Wereley, S. T., "A correlation-based continuous window-shift technique to reduce the peak-locking effect in digital PIV image evaluation", Experiments in Fluids, Vol.32, (2002), pp.506-517